ACS Catalysis

pubs.acs.org/acscatalysis Letter

Influence of Oxygen Vacancies and Surface Facets on Water Oxidation Selectivity toward Oxygen or Hydrogen Peroxide with $BiVO_4$

Pavle Nikačević, Franziska S. Hegner,* José Ramón Galán-Mascarós, and Núria López*

Cite This: *ACS Catal.* 2021, 11, 13416–13422 Read Online

ACCESS | Metrics & More | Article Recommendations | Supporting Information

ABSTRACT: Bismuth vanadate ($BiVO_4$) is one of the most promising photoanode materials for water oxidation. However, the water oxidation mechanism and selectivity on the different surfaces of $BiVO_4$ are still not well understood, partly because of the structural complexity introduced by the presence of oxygen vacancies in the material. Using density functional theory, we show that the (001) surface of $BiVO_4$ with subsurface vacancies is the most suitable for the oxygen evolution reaction, whereas the pristine (011) surface favors the hydrogen peroxide evolution reaction. A mechanism by which the vacancies can be removed from the surface, thereby influencing the water oxidation selectivity, is also described. Our results thus emphasize the crucial impact of the local structure on the catalytic selectivity in ternary oxides.

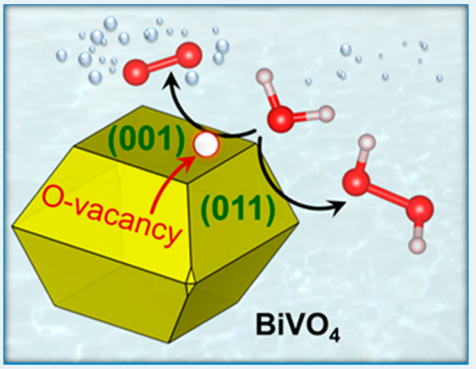

KEYWORDS: *bismuth vanadate, density functional theory, water oxidation, oxygen vacancies, selectivity, oxygen evolution reaction, hydrogen peroxide evolution*

In recent years, bismuth vanadate ($BiVO_4$) has become one of the most promising catalysts for photoelectrochemical water splitting.[1−3] It is a ternary oxide and an n-type semiconductor, which makes it suitable as a photoanode material for the oxygen evolution reaction (OER). $BiVO_4$ has a relatively low band gap of 2.4 eV and is inexpensive, nontoxic, and stable in aqueous solution.[4] In its monoclinic scheelite form, $BiVO_4$ has a remarkable half-cell solar-to-hydrogen theoretical efficiency of 8.1%.[5] However, its poor electron conductivity and slow water oxidation kinetics limit the use of nonmodified $BiVO_4$ as a practical OER catalyst.[1] In order to overcome these issues, various strategies to modify $BiVO_4$ photoanodes have been proposed.[6−8] Apart from OER, $BiVO_4$ also catalyzes the hydrogen peroxide evolution reaction (HPER)[9,10] in the presence of bicarbonate electrolyte or modified with different materials.[11−13] HPER has a standard electrode potential of 1.78 V vs standard hydrogen electrode (SHE),[14] and consumes water to produce H_2O_2. Current large-scale hydrogen peroxide production uses the anthraquinone oxidation process, which involves toxic precursors and various organic solvents.[15] An alternative means of production is highly desired,[16] as H_2O_2 has numerous applications: it is used as a bleaching agent or an oxidant and has various applications in the chemical industry, water treatment, metal processing, etc.[15,17] For photocatalytic HPER on $BiVO_4$ to be industrially viable, it needs to be better understood, particularly its selectivity with respect to the competitive OER.

One of the parameters important for the water oxidation performance on $BiVO_4$ is the exposed surface facet.[18] A nanocrystal of monoclinic scheelite $BiVO_4$ contains different surface facets, of which the (001) and (011)[19] surfaces comprise 99.3% of the nanocrystal's surface area (see Supporting Information for the detailed explanation).[20,21] These two facets were shown to lead to large anisotropies,[22−24] and their influence on the water oxidation mechanisms is considered in the present work.

On a different note, the $BiVO_4$ surfaces are not always pristine—they usually contain structural defects.[25] The most common type of defect in ternary oxide semiconductors are oxygen vacancies ($\mathcal{V}_o$).[26] Vacancies can improve a semiconductor's conductivity and charge separation efficiency by acting as shallow n-type donors.[27,28] They may also improve visible light absorption by reducing the band gap and improve the charge transfer between the material and the electrolyte (water).[29] Nonetheless, the $\mathcal{V}_o$s in semiconductors may be counterproductive for OER efficiency by acting as electron−

Received: July 20, 2021
Revised: September 26, 2021
Published: October 20, 2021

hole recombination centers[30,31] or by trapping photogenerated charge carriers or polarons and inhibiting charge transfer.[32,33] Several studies suggest that these disadvantageous effects arise from the oxygen vacancies formed in the bulk, while the advantageous effects arise from the vacancies formed on the surface of a semiconductor.[34−36] In $BiVO_4$, $\mathcal{V}_o$s significantly alter the geometric[37] and electronic[38−40] structure and thereby the water oxidation mechanism. However, their exact influence on water oxidation is not fully understood because studies are still limited and inconclusive.[40,41] Even though the vacancies may not be thermodynamically stable at the potentials necessary for water oxidation (see Supporting Information section 2.8 for analysis of the $\mathcal{V}_o$ formation energies and Pourbaix diagram), they are kinetically trapped, as experimental evidence shows,[42−44] and present in the material at high potentials. It was shown that the $BiVO_4$-based material with an exposed vacancy-rich (001) surface significantly improves photocatalytic water oxidation.[43] A theoretical study on this surface suggested that the surface oxygen vacancies increase the number of water splitting active sites and enhance hole transfer from the photoanode surface to the electrolyte.[29] In addition to that, it was shown that the vacancies lower the selectivity toward H_2O_2, therefore shifting the equilibrium toward OER.[44] The vacancies examined in these works arise when an oxygen atom from a VO_4^{3-} unit is removed and the two excess electrons remain in the cavity left by that atom, with no significant changes to the local structure. In this type of defect, the vacancy is effectively localized on a single vanadium atom, which is why we label it localized vacancy ($\mathcal{V}_o^{loc}$). The two additional electrons created by removing an O atom also remain localized at the vacancy site. This doubly occupied defect state is also called F-center.[26] Recently, however, we have shown that another, distinct type of oxygen vacancy (known as split vacancy, $\mathcal{V}_o^{split}$) could exist in the bulk and on the (001) surface of $BiVO_4$,[38] which was later also found by Wang et al.[27] In this type of defect, the local structure changes after the O atom is removed—atoms move in such a way that an oxygen atom from a neighboring VO_4^{3-} unit increases its coordination number by forming an oxo-bridge with the vanadium that lost an O atom. The vacancy is therefore divided (split) between two neighboring vanadium atoms, unlike $\mathcal{V}_o^{loc}$. In the bulk, the two types of vacancies have similar formation energies. However, on the (001) surface, $\mathcal{V}_o^{split}$ in the subsurface layer was found to be ∼1 eV more stable than $\mathcal{V}_o^{loc}$, with a quasi-barrierless transition to $\mathcal{V}_o^{split}$ (the energy barrier being 0.1 eV or less).[38] The two vacancy types also have distinct electronic structures. $\mathcal{V}_o^{loc}$ has a single, two-electron intragap state that lies deep within the band gap. The electrons are localized between the bismuth and vanadium atoms that share the vacancy, where the missing oxygen atom would be, reducing both Bi and V. $\mathcal{V}_o^{split}$ has two single-electron intragap states, one of which is deep and localized on a vanadium atom sharing the vacancy, while the other one is shallow (close to the conduction band) and may be delocalized over different V atoms. The vanadium atoms sharing the vacancy are reduced. As the electronic structure greatly affects catalytic mechanisms and selectivity by influencing the material's conductivity and charge separation efficiency, it is important to investigate the influence of these different kinds of vacancies on the water oxidation reaction.

We first studied the oxygen vacancy formation on the (011) surface and observed that, similarly to the (001) surface, a V−O−V bridge-forming $\mathcal{V}_o^{split}$ is preferred over $\mathcal{V}_o^{loc}$. Then, we modeled the OER and HPER reactions on the (001) and the (011) surfaces with and without a $\mathcal{V}_o^{split}$ in the subsurface, where the vacancy is the most stable. With these results, we obtained a complete picture of water oxidation on $BiVO_4$, elucidating its activity and selectivity with respect to different surface facets and the presence of oxygen vacancies on these surfaces. This allows for a better understanding of the fundamental nature of the water oxidation mechanisms on $BiVO_4$, which can guide the optimization and design of more efficient and selective photoanodes.

COMPUTATIONAL METHODS

Density functional theory (DFT) simulations were performed using the Vienna Ab initio Simulation Package (VASP)[45,46] and the PBEsol[47] exchange-correlation functional, as described in the Supporting Information. To calculate the electronic energy as a function of applied potential on selected systems, we carried out calculations with an implicit solvent model and a modified electrochemical potential by a surface-charging method based on the linearized Poisson−Boltzmann equation, as implemented in VASPsol.[48−50] This approach is also known as grand canonical DFT (GC-DFT), due to its grand canonical description of the electrons. We also carried out calculations with the PBE0[51] functional with 10% of exact exchange as a benchmark (see Supporting Information).[38] All of the structures are uploaded to the ioChem-BD database,[52,53] where they are openly accessible. Both (001) and (011) surfaces were modeled with similar, converged layer thicknesses, as shown in Figure 1. First, we modeled different types

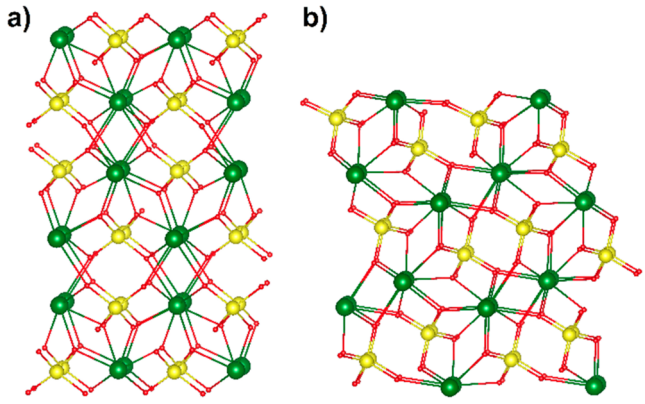

Figure 1. (a) Six-layered (001) surface slab and (b) three-layered (011) surface slab, as used in the calculations. One layer includes four $BiVO_4$ units for the (001) and eight $BiVO_4$ units for the (011) surface. Color code: Bi, V, and O are represented in green, yellow, and red, respectively (rendered with VESTA).[54]

of oxygen vacancies on the (011) surface, in order to find the most stable one. For this, we considered vacancies localized on 12 different positions in the slab, as well as two systems with a $\mathcal{V}_o^{split}$, as shown in the Supporting Information (Figure S1b).

Next, we investigated three distinct oxygen evolution reaction mechanistic pathways, as well as the pathway for H_2O_2 production, for the (001) and (011) surfaces, both pristine and with the most common vacancy type. The feasibility of the mechanisms was evaluated using the

https://doi.org/10.1021/acscatal.1c03256
ACS Catal. 2021, 11, 13416−13422

computational hydrogen electrode (CHE) approach, at the electrolyte pH 0 and 1 bar of H_2 in the gas phase at 298 K.[55] The CHE description accuracy of the most optimal mechanisms was confirmed at the GC-DFT level. Two pathways were found in the literature[24,56] as the most likely mechanisms on the pristine (001) and (011) surfaces (Figure 2a). The first pathway (referred to as OER pathway A, shown with blue arrows) was expected for the pristine (001) surface. Another mechanism (referred to as OER pathway B, shown with red arrows) was expected to happen on the pristine (011) surface. The main difference between these mechanisms is the peroxo-bridge between Bi and V atoms (intermediates **2a**−**4a**) that is present in pathway A, whereas pathway B includes an OOH group adsorbed to the surface (intermediates **3b** and **4b**).

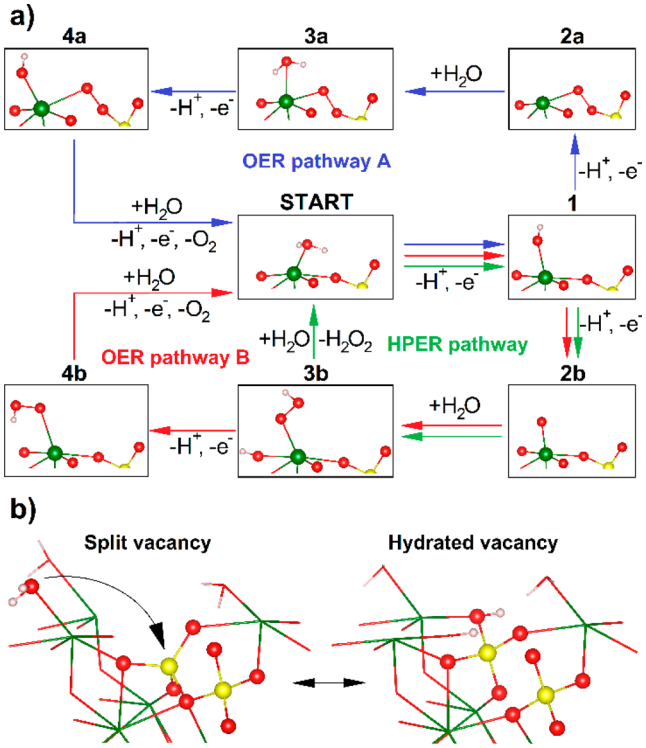

Figure 2. (a) Water oxidation mechanistic pathways on $BiVO_4$: OER pathway A, OER pathway B, and HPER pathway; (b) vacancy hydration.

With the systems containing oxygen vacancies, the vacancy creation/annihilation can be directly involved in the water oxidation mechanism.[57−59] This leads to the third OER mechanistic pathway, in which the vacancy is effectively filled by an oxygen atom coming from an adsorbed water molecule (Figure 2b). The resulting system is similar to the pristine surface, but it has two extra hydrogen atoms adsorbed, so it keeps the reduced oxidation state of the system with a vacancy; that is, it has two additional electrons. Such a system therefore contains a hydrated vacancy, which leads to a modified OER mechanism, referred to as OER pathway HV (see Supporting Information, section 2). Starting from a hydrated vacancy, the pristine surface is recovered after two hydrogen removals, and then, by evolving O_2, the vacancy is reintroduced (Figure S8).

The hydrogen peroxide evolution pathway (shown with green arrows in Figure 2a) starts in the same way as OER pathway B. Intermediate **3b**, included in both of these mechanisms, contains an OOH group in the proximity of a hydrogen atom. Instead of oxidizing this system to form the intermediate **4b**, hydrogen peroxide can be evolved from the system. Another possible HPER mechanism includes oxidation of a different water molecule of intermediate **1** and forming another OH group instead of the oxo group as in the intermediate **2b**. Two OH groups then combine directly into hydrogen peroxide. This mechanism is not considered here, as it is less efficient than the other pathway (see Supporting Information).

RESULTS

Regarding vacancies on the (011) surface of $BiVO_4$, we found two stable vacancy types: a localized vacancy, $\mathcal{V}_o^{loc}$, and a split vacancy, $\mathcal{V}_o^{split}$, as on the (001) surface.[38] $\mathcal{V}_o^{split}$ was ∼0.6 eV more stable than $\mathcal{V}_o^{loc}$, and both systems have an analogous electronic structure to their (001) surface counterparts (see Supporting Information, section 2). Systems with $\mathcal{V}_o^{loc}$ have a deep intragap state with the extra electrons being paired and, therefore, no net magnetization. In the systems with $\mathcal{V}_o^{split}$, the electrons are no longer paired, and the system has a net magnetization of two.

We first analyzed the OER on the (001) surface with a $\mathcal{V}_o^{split}$ between the first two layers (Figure S1a), along with the pristine surface for comparison. The efficiency of different mechanisms can be evaluated by comparing their thermodynamic overpotentials (η_{TD}). The overpotential is calculated from the energy of the reaction step with the highest energy, namely the potential-determining step (PDS) and the equilibrium potential of the reaction. Steps that do not include transfer of charged particles are grouped together with the appropriate proton-coupled electron transfer (PCET), so that four PCET steps are obtained as in the CHE formalism.[55] The energy differences for each reaction step are presented in the Supporting Information (section 3). From these data, the reaction profiles are plotted (Figures 3 and S10). The mechanism proposed in the literature for the pristine (001) surface (OER pathway A, in blue) is significantly less efficient (η_{TD} = 1.2 V) than the mechanism happening on the (001) surface with $\mathcal{V}_o^{split}$ (following OER pathway B, in red, η_{TD} = 0.4 V). The oxygen vacancy particularly impacts the first PCET step, which is the PDS for the pristine system, lowering its energy by almost 2 eV. This step consists of a hydrogen removal, which is more efficient in all of the reaction steps happening on a surface with a vacancy (see Supporting Information, section 3). The subsurface vacancy introduces additional electrons which lie in high-energy states within the band gap and which are easily removed,[38] therefore facilitating the PCET. Hence, the subsurface split vacancies enhance OER efficiency on the (001) surface, similarly to what was found for vacancies localized in the surface layer.[29] This is also in agreement with recent experimental data, showing that vacancy-rich (001) surfaces significantly improve OER efficiency[43] and favor oxygen evolution kinetics.[60] As the adsorption of water enables vacancy hydration, a system with such a vacancy was also considered. Such a system was 0.09 eV more stable than the system with a nonhydrated, $\mathcal{V}_o^{split}$. From this energy difference, it can be calculated that 97% of the vacancies on the (001) surface are hydrated (see Supporting

https://doi.org/10.1021/acscatal.1c03256
ACS Catal. 2021, 11, 13416−13422

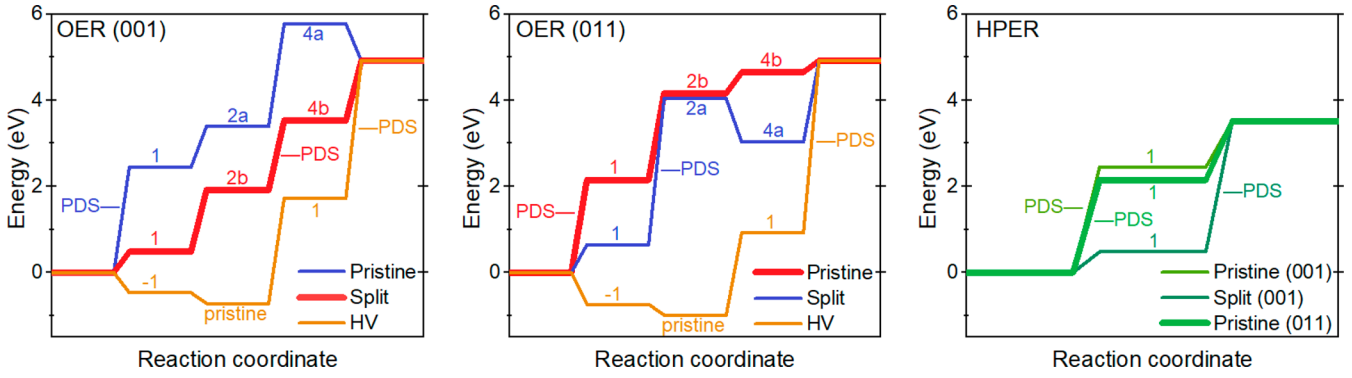

Figure 3. Gibbs free energy profile of water oxidation on $BiVO_4$ (some steps are merged so that the resulting steps all include a PCET). Blue, OER pathway A; red, OER pathway B; brown, OER pathway HV; green, HPER pathway. The most optimal mechanism for each case (the lowest PDS) is represented with a thicker line.

Information). This implies that most of the subsurface vacancies tend to become hydrated when the $BiVO_4$ electrode is immersed in water. The OER mechanism with a hydrated vacancy, pathway HV (shown in brown), is not efficient on this surface because of its last two reaction steps, which correspond to a single PCET step (η_{TD} = 2.0 V). In this step, the vacancy is reintroduced into the surface, which has a high cost in energy (Figure S8). However, the first two PCET steps of these pathways (oxidation of the hydrated vacancy) are thermodynamically favorable.

For OER on the (011) surface, an analogous set of calculations was performed, and energy differences for each reaction step are presented in the Supporting Information (section 3). The corresponding reaction profiles are shown in Figures 3 and S11. The mechanism proposed in the literature for the pristine (011) surface (OER pathway B, shown in red) is the most efficient, with the second step being potential determining (η_{TD} = 0.9 V). With respect to the pristine surface, the OER efficiency is reduced when the vacancy is introduced (shown in blue, η_{TD} = 2.2 V), in contrast to what was found for the (001) surface. Again, we considered the possibility of vacancy hydration. The system containing a hydrated vacancy was 0.20 eV less stable than the system with a nonhydrated (split) vacancy. From this difference, it can be estimated that the amount of hydrated vacancies on the (011) surface is approximately 0.05%, which is negligible compared to their amount on the (001) surface (97%), where vacancy hydration was found to be thermodynamically favored. Analogously to what was found for the (001) surface, OER on the (011) surface with hydrated vacancy, pathway HV (shown in brown), is inefficient because of its last PCET step (η_{TD} = 2.8 V), while the first two steps (i.e., the oxidation of the hydrated vacancy) are thermodynamically favorable.

For the HPER, there are four systems in total to consider: the (001) and (011) surfaces, both pristine and with a $\mathcal{V}_o^{split}$ (Figures 3 and S12). For the (011) surface with a $\mathcal{V}_o^{split}$, the relevant intermediate (**2b**) could not be stabilized, and the HPER on this system is considered in the Supporting Information (section 3). Out of the remaining three systems, the preferred mechanism takes place on the pristine (011) surface, with the first step being the PDS. Its overpotential η_{TD} is equal to 0.4 V. We would like to note that Siahrostami et al. found a favorable η_{TD} of 0.2 V for HPER on the (111) surface,[61] where we would expect a higher HPER activity. However, if we consider the equilibrium nanoparticle shape coming from the Wulff construction, the (111) surface represents a minor fraction of the total area (less than 1%, see Supporting Information, section 2.1).[21] Therefore, we kept the two most stable surfaces in our analysis.

For completeness, to confirm the accuracy of the used CHE approach and the PBEsol functional, we also performed calculations with GC-DFT at constant applied potentials and with a modified PBE0 functional with 10% exact exchange, respectively (see Supporting Information, sections 3.5 and 3.6). For the surface-charging method (GC-DFT), we took into account only the PDS of the two favored reactions (OER on the (001) surface with vacancy and HPER on the pristine (011) surface) at an applied potential of 1.6 V (vs SHE). This is the equilibrium potential of the former reaction at the CHE level. The energy of the PDS changes by less than 0.2 eV compared to the CHE approach at constant charge (Figure S16), therefore supporting the adequacy of our method. Similarly, using a hybrid functional for OER on the (001) surface with vacancy did not significantly alter the water oxidation energies (Figure S17).

So far, we have compared different mechanisms on the same surface; now, we compare the most suitable reaction mechanisms between different surfaces (Figure 4). In order

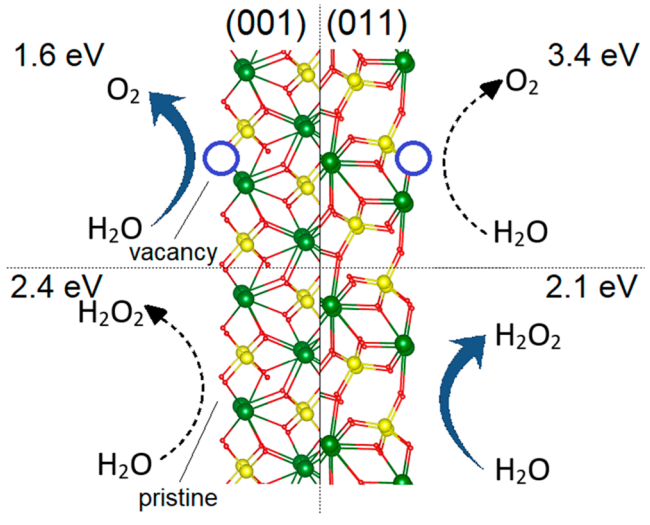

Figure 4. Most advantageous water oxidation reactions on $BiVO_4$ with the energies of their respective potential-determining steps. Two favorable processes are represented with a thicker arrow.

https://doi.org/10.1021/acscatal.1c03256
ACS Catal. 2021, 11, 13416−13422

to elucidate the water oxidation selectivity, we compare the PDS energies directly instead of the overpotentials, as OER and HPER have different equilibrium potentials. Comparing OER on the (001) and (011) surfaces, we see that OER happens more easily on the (001) surface, as the PDS is lower in energy (1.6 eV, surface with vacancy) than on the (011) surface (2.1 eV, pristine surface). Both of these reactions follow the pathway B, so we conclude that the pathway A does not happen on $BiVO_4$ in the presence of oxygen vacancies. The OER on the (001) surface with $\mathcal{V}_o^{split}$ is also the overall most favorable water oxidation reaction on all of the systems considered, increasing by less than 0.2 eV at an applied potential of 1.6 V (Figure S16a). The second most energetically favorable reaction is HPER on the pristine (011) surface with the PDS of 2.1 eV (which decreased by only ∼0.1 eV at an applied potential of 1.6 V, Figure S16b). This reaction has the equivalent PDS as the OER on the same surface. However, the second PCET step that ultimately produces hydrogen peroxide (1.4 eV) is lower in energy than the second PCET step of the OER reaction, which stops at the intermediate **2b** formation (2.0 eV). This implies that the (011) surface is more favorable for HPER than for OER. The results also suggest that oxygen vacancies in the subsurface favor oxygen evolution, whereas HPER is more favorable on the pristine material. Our theoretical prediction explains recent experiments,[44] showing that V_2O_5-treated $BiVO_4$, which has a lower amount of oxygen vacancies than the pristine material, favors HPER over OER.

It is known that bicarbonate is needed as the electrolyte for an efficient H_2O_2 evolution reaction on $BiVO_4$.[9,11,13] We propose that the bicarbonate ions may have a role in detrapping vacancies by lowering the barrier for vacancy hydration, as the oxygen vacancies are not thermodynamically stable at the potentials needed for water oxidation (they are only present because they are kinetically trapped). Consequently, removing the vacancies from the surface would shift the selectivity toward H_2O_2. However, this hypothesis would need to be tested by further calculations and experiments.

In conclusion, by modeling all of the reaction intermediates for different water oxidation mechanisms, we have shown that the most favorable electrochemical process on $BiVO_4$ is the OER on the (001) surface with a subsurface $\mathcal{V}_o^{split}$. The most energetically demanding proton-coupled electron transfer step for this reaction has an energy of 1.6 eV (η_{TD} = 0.4 V). The second most favorable process is hydrogen peroxide evolution reaction on the pristine (011) surface, with the most energetically demanding PCET step being 2.1 eV (η_{TD} = 0.4 V). Therefore, if no oxygen vacancies are present in the material, HPER on the (011) surface becomes the most favorable reaction. We have also shown that it is thermodynamically favored to fill oxygen vacancies on the (001) surface with a water molecule (vacancy hydration), which can further influence the photocatalytic activity of $BiVO_4$ by changing the number of split vacancies on its surface. Our results highlight the crucial impact of oxygen vacancies, not only on the catalytic activity but also on the water oxidation selectivity on ternary metal oxides. By controlling the exposed surface facet and the vacancy content, selectivity can be driven toward either OER or HPER, which is important for the design of novel photoelectrodes.

■ ASSOCIATED CONTENT

Supporting Information

The Supporting Information is available free of charge at https://pubs.acs.org/doi/10.1021/acscatal.1c03256.

Computational methods, vacancy formation energies, water oxidation intermediate energies, densities of states, GC-DFT energies, vibrational frequencies (PDF)

■ AUTHOR INFORMATION

Corresponding Authors

Franziska S. Hegner − *Institut Català d'Investigació Química (ICIQ), The Barcelona Institute of Science and Technology (BIST), 43007 Tarragona, Spain;* Present Address: Technical University of Munich (TUM), James-Franck-Straße 1, 85748 Garching, Germany; Email: fhegner@iciq.es

Núria López − *Institut Català d'Investigació Química (ICIQ), The Barcelona Institute of Science and Technology (BIST), 43007 Tarragona, Spain;* orcid.org/0000-0001-9150-5941; Email: nlopez@iciq.es

Authors

Pavle Nikačević − *Institut Català d'Investigació Química (ICIQ), The Barcelona Institute of Science and Technology (BIST), 43007 Tarragona, Spain*

José Ramón Galán-Mascarós − *Institut Català d'Investigació Química (ICIQ), The Barcelona Institute of Science and Technology (BIST), 43007 Tarragona, Spain; Catalan Institution for Research and Advanced Studies (ICREA), 08010 Barcelona, Spain;* orcid.org/0000-0001-7983-9762

Complete contact information is available at: https://pubs.acs.org/10.1021/acscatal.1c03256

Author Contributions

All authors have given approval to the final version of the manuscript.

Notes

The authors declare no competing financial interest.

■ ACKNOWLEDGMENTS

We thank Dr. Stephan Steinmann for generously providing us help related to GC-DFT and symmetrizing our slabs. This work was funded by European Union's Horizon 2020 project SOLAR2CHEM (Grant Agreement No. 861151). We also thank BSC-RES for providing generous computational resources.

■ ABBREVIATIONS

DFT, density functional theory; OER, oxygen evolution reaction; HPER, hydrogen peroxide evolution reaction; GC, Grand-Canonical; PCET, proton-coupled electron transfer; PDS, potential-determining step

■ REFERENCES

(1) Tayebi, M.; Lee, B. Recent Advances in $BiVO_4$ Semiconductor Materials for Hydrogen Production Using Photoelectrochemical Water Splitting. *Renewable Sustainable Energy Rev.* **2019**, *111*, 332−343.

(2) Malathi, A.; Madhavan, J.; Ashokkumar, M.; Arunachalam, P. A Review on $BiVO_4$ Photocatalyst: Activity Enhancement Methods for Solar Photocatalytic Applications. *Appl. Catal., A* **2018**, *555*, 47−74.

(3) Kudo, A.; Ueda, K.; Kato, H.; Mikami, I. Photocatalytic O_2 Evolution Under Visible Light Irradiation on $BiVO_4$ in Aqueous $AgNO_3$ Solution. *Catal. Lett.* **1998**, *53*, 229−230.
(4) Jia, Q.; Iwashina, K.; Kudo, A. Facile Fabrication of an Efficient $BiVO_4$ Thin Film Electrode for Water Splitting Under Visible Light Irradiation. *Proc. Natl. Acad. Sci. U. S. A.* **2012**, *109* (29), 11564−11569.
(5) Pihosh, Y.; Turkevych, I.; Mawatari, K.; Uemura, J.; Kazoe, Y.; Kosar, S.; Makita, K.; Sugaya, T.; Matsui, T.; Fujita, D.; Tosa, M.; Kondo, M.; Kitamori, T. Photocatalytic Generation of Hydrogen by Core-Shell WO_3/$BiVO_4$ Nanorods with Ultimate Water Splitting Efficiency. *Sci. Rep.* **2015**, *5*, 11141.
(6) Kim, J.; Lee, J. Elaborately Modified $BiVO_4$ Photoanodes for Solar Water Splitting. *Adv. Mater.* **2019**, *31* (20), 1806938.
(7) Chen, L.; Alarcon-Llado, E.; Hettick, M.; Sharp, I.; Lin, Y.; Javey, A.; Ager, J. Reactive Sputtering of Bismuth Vanadate Photoanodes for Solar Water Splitting. *J. Phys. Chem. C* **2013**, *117* (42), 21635−21642.
(8) Tayebi, M.; Tayyebi, A.; Lee, B. Improved Photoelectrochemical Performance of Molybdenum (Mo)-Doped Monoclinic Bismuth Vanadate with Increasing Donor Concentration. *Catal. Today* **2019**, *328*, 35−42.
(9) Fuku, K.; Sayama, K. Efficient Oxidative Hydrogen Peroxide Production and Accumulation in Photoelectrochemical Water Splitting Using a Tungsten Trioxide/Bismuth Vanadate Photoanode. *Chem. Commun.* **2016**, *52*, 5406−5409.
(10) Shi, X.; Siahrostami, S.; Li, G.; Zhang, Y.; Chakthranont, P.; Studt, F.; Jaramillo, T.; Zheng, X.; Norskov, J. Understanding Activity Trends in Electrochemical Water Oxidation to Form Hydrogen Peroxide. *Nat. Commun.* **2017**, *8*, 701.
(11) Shi, X.; Zhang, Y.; Siahrostami, S.; Zheng, X. Light-Driven $BiVO_4$ Fuel Cell with Simultaneous Production of H_2O_2. *Adv. Energy Mater.* **2018**, *8*, 1801158.
(12) Miyase, Y.; Takasugi, S.; Iguchi, S.; Miseki, Y.; Gunji, T.; Sasaki, K.; Fujita, E.; Sayama, K. Modification of $BiVO_4$/WO_3 Composite Photoelectrodes with Al_2O_3 via Chemical Vapor Deposition for Highly Efficient Oxidative H_2O_2 Production from H_2O. *Sustain. Energy Fuels* **2018**, *2*, 1621−1629.
(13) Fuku, K.; Miyase, Y.; Miseki, Y.; Gunji, T.; Sayama, K. Enhanced Oxidative Hydrogen Peroxide Production on Conducting Glass Anodes Modified with Metal Oxides. *ChemistrySelect* **2016**, *1* (18), 5721−5726.
(14) https://www.h2o2.com/technical-library/physical-chemical-properties/thermodynamic-properties/default.aspx?pid=50&name=Standard-Electrode-Potentials (accessed 2021-08-25).
(15) Campos-Martin, J. M.; Blanco-Brieva, G.; Fierro, J. L. G. Hydrogen Peroxide Synthesis: An Outlook beyond the Anthraquinone Process. *Angew. Chem., Int. Ed.* **2006**, *45* (42), 6962−6984.
(16) Siahrostami, S.; Verdaguer-Casadevall, A.; Karamad, M.; Deiana, D.; Malacrida, P.; Wickman, B.; Escudero-Escribano, M.; Paoli, E. A.; Frydendal, R.; Hansen, T. W.; Chorkendorff, I.; Stephens, I. E. L.; Rossmeisl, J. Enabling Direct H_2O_2 Production Through Rational Electrocatalyst Design. *Nat. Mater.* **2013**, *12*, 1137−1143.
(17) Hage, R.; Lienke, A. Applications of Transition-Metal Catalysts to Textile and Wood-Pulp Bleaching. *Angew. Chem., Int. Ed.* **2006**, *45* (2), 206−222.
(18) Lardhi, S.; Cavallo, L.; Harb, M. Significant Impact of Exposed Facets on the $BiVO_4$ Material Performance for Photocatalytic Water Splitting Reactions. *J. Phys. Chem. Lett.* **2020**, *11* (14), 5497−5503.
(19) In the present work, the (001), (011), (101), and (111) surfaces are labeled in the body-centered *I*2/*b* setting, which is convenient for computations. In the literature, they are often labeled in the conventional *C*2/*c* setting, as (010), $(\bar{1}11)$, $(\bar{1}10)$, and (011), respectively.[21]
(20) Sleight, A.; Chen, H.; Ferretti, A.; Cox, D. Crystal growth and structure of $BiVO_4$. *Mater. Res. Bull.* **1979**, *14* (12), 1571−1581.
(21) Li, G. First-Principles Investigation of the Surface Properties of Fergusonite-Type Monoclinic $BiVO_4$ Photocatalyst. *RSC Adv.* **2017**, *7* (15), 9130−9140.
(22) Li, R.; Zhang, F.; Wang, D.; Yang, J.; Li, M.; Zhu, J.; Zhou, X.; Han, H.; Li, C. Spatial Separation of Photogenerated Electrons and Holes Among {010} and {110} Crystal Facets of $BiVO_4$. *Nat. Commun.* **2013**, *4*, 1432.
(23) Liu, T.; Zhou, X.; Dupuis, M.; Li, C. The Nature of Photogenerated Charge Separation Among Different Crystal Facets of $BiVO_4$ Studied by Density Functional Theory. *Phys. Chem. Chem. Phys.* **2015**, *17* (36), 23503−23510.
(24) Hu, J.; Chen, W.; Zhao, S.; Su, H.; Chen, Z. Anisotropic Electronic Characteristics, Adsorption, and Stability of Low-Index $BiVO_4$ Surfaces for Photoelectrochemical Applications. *ACS Appl. Mater. Interfaces* **2018**, *10* (6), 5475−5484.
(25) Lee, D.; Wang, W.; Zhou, C.; Tong, X.; Liu, M.; Galli, G.; Choi, K. The Impact of Surface Composition on the Interfacial Energetics and Photoelectrochemical Properties of $BiVO_4$. *Nat. Energy* **2021**, *6*, 287−294.
(26) Daelman, N.; Hegner, F. S.; Rellan-Pineiro, M.; Capdevila-Cortada, M.; Garcia-Muelas, R.; Lopez, N. Quasi-Degenerate States and Their Dynamics in Oxygen Deficient Reducible Metal Oxides. *J. Chem. Phys.* **2020**, *152*, 050901.
(27) Wang, S.; Chen, P.; Bai, Y.; Yun, J.; Liu, G.; Wang, L. New $BiVO_4$ Dual Photoanodes with Enriched Oxygen Vacancies for Efficient Solar-Driven Water Splitting. *Adv. Mater.* **2018**, *30* (20), 1800486.
(28) Zhang, W.; Song, L.; Cen, J.; Liu, M. Mechanistic Insights into Defect-Assisted Carrier Transport in Bismuth Vanadate Photoanodes. *J. Phys. Chem. C* **2019**, *123* (34), 20730−20736.
(29) Hu, J.; Zhao, X.; Chen, W.; Su, H.; Chen, Z. Theoretical Insight into the Mechanism of Photoelectrochemical Oxygen Evolution Reaction on $BiVO_4$ Anode with Oxygen Vacancy. *J. Phys. Chem. C* **2017**, *121* (34), 18702−18709.
(30) Freysoldt, C.; Grabowski, B.; Hickel, T.; Neugebauer, J.; Kresse, G.; Janotti, A.; Van de Walle, C. First-Principles Calculations for Point Defects in Solids. *Rev. Mod. Phys.* **2014**, *86*, 253−305.
(31) Cheng, C.; Fang, Q.; Fernandez-Alberti, S.; Long, R. Controlling Charge Carrier Trapping and Recombination in $BiVO_4$ with the Oxygen Vacancy Oxidation State. *J. Phys. Chem. Lett.* **2021**, *12*, 3514−3521.
(32) Selim, S.; Pastor, E.; Garcia-Tecedor, M.; Morris, M.; Francas, L.; Sachs, M.; Moss, B.; Corby, S.; Mesa, C.; Gimenez, S.; Kafizas, A.; Bakulin, A.; Durrant, J. Impact of Oxygen Vacancy Occupancy on Charge Carrier Dynamics in $BiVO_4$ Photoanodes. *J. Am. Chem. Soc.* **2019**, *141* (47), 18791−18798.
(33) Qiu, W.; Xiao, S.; Ke, J.; Wang, Z.; Tang, S.; Zhang, K.; Qian, W.; Huang, Y.; Huang, D.; Tong, Y.; Yang, S. Freeing the Polarons to Facilitate Charge Transport in $BiVO_4$ from Oxygen Vacancies with an Oxidative 2D Precursor. *Angew. Chem., Int. Ed.* **2019**, *58* (52), 19087−19095.
(34) Zhao, X.; Hu, J.; Yao, X.; Chen, S.; Chen, Z. Clarifying the Roles of Oxygen Vacancy in W-Doped $BiVO_4$ for Solar Water Splitting. *ACS Appl. Energy Mater.* **2018**, *1*, 3410−3419.
(35) Fernandez-Climent, R.; Gimenez, S.; Garcia-Tecedor, M. The Role of Oxygen Vacancies in Water Splitting Photoanodes. *Sustain. Energy Fuels* **2020**, *4*, 5916−5926.
(36) Wang, Z.; Mao, X.; Chen, P.; Xiao, M.; Monny, S.; Wang, S.; Konarova, M.; Du, A.; Wang, L. Understanding the Roles of Oxygen Vacancies in Hematite-Based Photoelectrochemical Processes. *Angew. Chem., Int. Ed.* **2019**, *58* (4), 1030−1034.
(37) Osterbacka, N.; Wiktor, J. Influence of Oxygen Vacancies on the Structure of $BiVO_4$. *J. Phys. Chem. C* **2021**, *125*, 1200−1207.
(38) Hegner, F. S.; Forrer, D.; Galan-Mascaros, J. R.; Lopez, N.; Selloni, A. Versatile Nature of Oxygen Vacancies in Bismuth Vanadate Bulk and (001) Surface. *J. Phys. Chem. Lett.* **2019**, *10* (21), 6672−6678.
(39) Wang, W.; Strohbeen, P.; Lee, D.; Zhou, C.; Kawasaki, J.; Choi, K.; Liu, M.; Galli, G. The Role of Surface Oxygen Vacancies in $BiVO_4$. *Chem. Mater.* **2020**, *32*, 2899−2909.
(40) Seo, H.; Ping, Y.; Galli, G. Role of Point Defects in Enhancing the Conductivity of $BiVO_4$. *Chem. Mater.* **2018**, *30* (21), 7793−7802.

https://doi.org/10.1021/acscatal.1c03256
ACS Catal. 2021, 11, 13416−13422

(41) Cooper, J.; Scott, S.; Ling, Y.; Yang, J.; Hao, S.; Li, Y.; Toma, F.; Stutzmann, M.; Lakshmi, K.; Sharp, I. Role of Hydrogen in Defining the n-Type Character of $BiVO_4$ Photoanodes. *Chem. Mater.* **2016**, *28* (16), 5761−5771.
(42) Wang, S.; Chen, P.; Yun, J.; Hu, Y.; Wang, L. An Electrochemically Treated $BiVO_4$ Photoanode for Efficient Photoelectrochemical Water Splitting. *Angew. Chem., Int. Ed.* **2017**, *56* (29), 8500−8504.
(43) Hu, J.; He, H.; Zhou, X.; Li, Z.; Shen, Q.; Luo, W.; Alsaedi, A.; Hayat, T.; Zhou, Y.; Zou, Z. $BiVO_4$ Tubular Structures: Oxygen Defect-Rich and Largely Exposed Reactive {010} Facets Synergistically Boost Photocatalytic Water Oxidation and Selective N═N Coupling Reaction of 5-Amino-1H-Tetrazole. *Chem. Commun.* **2019**, *55* (39), 5635−5638.
(44) Wang, L.; Lu, Y.; Han, N.; Dong, C.; Lin, C.; Lu, S.; Min, Y.; Zhang, K. Suppressing Water Dissociation via Control of Intrinsic Oxygen Defects for Awakening Solar H_2O-to-H_2O_2 Generation. *Small* **2021**, *17*, 2100400.
(45) Kresse, G.; Furthmüller, J. Efficient Iterative Schemes for *Ab Initio* Total-Energy Calculations Using a Plane-Wave Basis Set. *Phys. Rev. B: Condens. Matter Mater. Phys.* **1996**, *54*, 11169−11186.
(46) Kresse, G.; Joubert, D. From Ultrasoft Pseudopotentials to the Projector Augmented-Wave Method. *Phys. Rev. B: Condens. Matter Mater. Phys.* **1999**, *59*, 1758−1775.
(47) (a) Perdew, J. P.; Ruzsinszky, A.; Csonka, G.; Vydrov, O.; Scuseria, G.; Constantin, L.; Zhou, X.; Burke, K. Restoring the Density-Gradient Expansion for Exchange in Solids and Surfaces. *Phys. Rev. Lett.* **2008**, *100*, 136406; Erratum. *Phys. Rev. Lett.* **2009**, *102*, 039902.
(48) Mathew, K.; Sundararaman, R.; Letchworth-Weaver, K.; Arias, T. A.; Hennig, R. G. Implicit Solvation Model for Density-Functional Study of Nanocrystal Surfaces and Reaction Pathways. *J. Chem. Phys.* **2014**, *140*, 084106.
(49) https://github.com/henniggroup/VASPsol (accessed 2021-08-25).
(50) Mathew, K.; Kolluru, V.; Mula, S.; Steinmann, S.; Hennig, R. Implicit Self-Consistent Electrolyte Model in Plane-Wave Density-Functional Theory. *J. Chem. Phys.* **2019**, *151*, 234101.
(51) Perdew, J. P.; Ernzerhof, M.; Burke, K. Rationale for Mixing Exact Exchange with Density Functional Approximations. *J. Chem. Phys.* **1996**, *105*, 9982−9985.
(52) Alvarez-Moreno, M.; de Graaf, C.; Lopez, N.; Maseras, F.; Poblet, J. M.; Bo, C. Managing the Computational Chemistry Big Data Problem: The ioChem-BD Platform. *J. Chem. Inf. Model.* **2015**, *55*, 95−103.
(53) Nikačević, P. DOI: 10.19061/iochem-bd-1-203 (accessed 2021-09-30).
(54) Momma, K.; Izumi, F. *VESTA*: A Three-Dimensional Visualization System for Electronic and Structural Analysis. *Appl. Crystallogr.* 2008, *41*, 653−658.
(55) Norskov, J.; Rossmeisl, J.; Logadottir, A.; Lindqvist, L.; Kitchin, J.; Bligaard, T.; Jonsson, H. Origin of the Overpotential for Oxygen Reduction at a Fuel-Cell Cathode. *J. Phys. Chem. B* **2004**, *108* (46), 17886−17892.
(56) Yang, J.; Wang, D.; Zhou, X.; Li, C. A Theoretical Study on the Mechanism of Photocatalytic Oxygen Evolution on $BiVO_4$ in Aqueous Solution. *Chem. - Eur. J.* **2013**, *19* (4), 1320−1326.
(57) Mefford, J.; Rong, X.; Abakumov, A.; Hardin, W.; Dai, S.; Kolpak, A.; Johnston, K.; Stevenson, K. Water Electrolysis on $La_{1-x}Sr_xCoO_{3-\delta}$ Perovskite Electrocatalysts. *Nat. Commun.* **2016**, *7*, 11053.
(58) Rong, X.; Parolin, J.; Kolpak, A. A Fundamental Relationship between Reaction Mechanism and Stability in Metal Oxide Catalysts for Oxygen Evolution. *ACS Catal.* **2016**, *6* (2), 1153−1158.
(59) Grimaud, A.; Diaz-Morales, O.; Han, B.; Hong, W.; Lee, Y.; Giordano, L.; Stoerzinger, K.; Koper, M.; Shao-Horn, Y. Activating Lattice Oxygen Redox Reactions in Metal Oxides to Catalyse Oxygen Evolution. *Nat. Chem.* **2017**, *9*, 457−465.
(60) Kahraman, A.; Vishlaghi, M.; Baylam, I.; Ogasawara, H.; Sennaroglu, A.; Kaya, S. The Fast-Track Water Oxidation Channel on $BiVO_4$ Opened by Nitrogen Treatment. *J. Phys. Chem. Lett.* **2020**, *11* (20), 8758−8764.
(61) Siahrostami, S.; Li, G.; Viswanathan, V.; Norskov, J. One- or Two-Electron Water Oxidation, Hydroxyl Radical, or H_2O_2 Evolution. *J. Phys. Chem. Lett.* **2017**, *8* (6), 1157−1160.

https://doi.org/10.1021/acscatal.1c03256
ACS Catal. 2021, 11, 13416−13422